AMS Home   Journals Home   Journal Archive   Subscribe   For Authors   Help   Advanced Search   Search [Go]

Full Text View

Internal Wave Interactions with Equatorial Deep Jets. Part I: Momentum-Flux Divergences

Joanna E. Muench

Seattle, Washington

Eric Kunze

Department of Oceanography, University of Washington, Seattle, Washington

ABSTRACT

Equatorial deep jets are an unsolved mystery of the equatorial oceans. These alternating zonal currents appear steady over time spans of years, but no postulated energy source has proven plausible, and elevated turbulent dissipation in the jets does not appear to erode them. Transfer of energy between the internal wave field and mean flow can occur through momentum-flux divergences, which could act to maintain the jets. Using a Garrett–Munk spectrum adjusted to the equator, the authors estimate the momentum-flux divergence from internal waves encountering critical layers in deep jets. The net momentum-flux divergences are sensitive to the rate at which wave–wave interactions replenish the internal wave spectrum depleted by critical-layer interactions with adjacent jets. Order-of-magnitude arguments indicate that even modest momentum-flux divergences could dramatically impact the mean flow.

1. Introduction

The equatorial deep jets remain an enigma of the equatorial circulation. These alternating east–west currents appear steady over 2-yr time spans, with little apparent vertical propagation (Firing 1987). Elevated dissipation rates are observed in the high shear zones between the jets (Gregg et al. 1995) but do not appear to erode the jets. The jets span the entire Pacific basin (Wijffels 1993; Hayes and Milburn 1980) and also appear in the Indian (Luyten and Swallow 1976; O'Neill and Luyten 1984) and Atlantic Oceans (Ponte et al. 1990).

The deep equatorial ocean is also a region of elevated internal wave activity. The low Coriolis frequency broadens the internal wave band, so there is more internal wave energy than at midlatitudes (Eriksen 1980). Observations show equatorial spectral levels are elevated over midlatitude by factors of 3–5. Waves with short vertical wavelengths are likely to encounter critical layers within the deep jets, creating both momentum-flux divergences that accelerate/decelerate the mean flow, and energy-flux divergences that elevate the dissipation rates over background deep ocean levels.

In this paper, we estimate the momentum- and energy-flux divergences associated within internal waves reaching critical layers with the deep jets and discuss their impact on the mean flow. We find that the spectral replenishment rate and vertical wavelength of the jets drastically alters our results. To understand the implications of our model, we estimate the magnitude of forcing for the deep jets expected from the calculated momentum-flux divergence. A complete analysis of acceleration of the deep jets due to internal wave momentum-flux divergence is presented by Muench and Kunze (1999, manuscript submitted to *J. Phys. Oceanogr.,* hereafter MK99).

In this introduction, we discuss previous attempts to estimate the momentum-flux divergence and present observational descriptions of the deep jets and internal wave field to be used in this model. In addition, we briefly discuss (i) how energy is transferred to the mean flow at critical layers and (ii) spectral replenishment of the internal wave spectrum due to wave–wave interactions. In section 2, we define various parameters required for our model of a GM spectrum of internal waves interacting with the deep jets; the model itself is developed in section 3. In section 4 we find that spectral replenishment by wave–wave interactions between and within the jets is necessary to explain the observed elevated dissipation rates. In section 5, we summarize our results and discuss some implications for the deep jets.

a. Previous estimates

Estimates of momentum-flux divergences arising from a sheared mean flow have been made for over a century. Reynolds (1895) first suggested parameterizing the momentum-flux divergence as an eddy viscosity

$$\langle u'w' \rangle = -\nu \frac{\partial U}{\partial z}, \qquad (1)$$

an approach widely used by oceanographers. However, if the momentum-flux divergence is due to critical layer interactions, this parameterization is not correct as it assumes a viscous decay. Based on a model of internal waves reaching critical layers at progressively increasing mean zonal velocity, Ruddick and Joyce (1979) parameterized the momentum-flux divergence due to downward-propagating waves in increasing shear as

$$\frac{\partial}{\partial z}\langle u'w' \rangle \approx -C_{uw} \frac{\partial U}{\partial z}, \qquad (2)$$

where $C_{uw} \approx 3 \times 10^{-5}$ m s^{-1}. Kunze and Müller (1989) used a similar parameterization in their model of internal waves accelerating a mean sheared flow and noted that (2) is analogous to a pseudo vertical velocity that acts on the mean shear but not the mean stratification.

Our study describes the momentum-flux divergence due to an isotropic wave spectrum interacting with the complicated geometry of the deep jets. While simple parameterizations may be correct in the presence of a surface-generated internal wave field where most energy is downward propagating, in the deep ocean the internal wave field is vertically symmetric. An entirely isotropic wave field has no net momentum-flux divergence associated with it; therefore, the geometry of the jets must determine the magnitude of the momentum-flux divergence.

b. Equatorial deep jets

Observations of jetlike features have been made in the equatorial Indian (Luyten and Swallow 1976; O'Neill and Luyten 1984) and Atlantic (Ponte et al. 1990) Oceans. The jets in the Pacific Ocean are the best documented. The deep Atlantic currents appear to have longer vertical scales than the Pacific jets (Ponte et al;K. Polzin 1996, personal communication); the effects of longer vertical wavelengths on the momentum-flux divergence are explored.

The jets are a persistent feature of the deep equatorial Pacific (Firing 1987). They are characterized by vertically alternating zonal currents centered on the equator with an average vertical wavelength of 330 m. The jets span 500- to 2000-m depth and are confined within 1° of the equator with an approximately Gaussian meridional shape (Firing 1987). While instantaneous zonal velocities of up to 20 cm s^{-1} have been observed, the maximum 16-month mean zonal velocity is 5 cm s^{-1} (Fig. 1). Individual observations of the jets span the equatorial Pacific from 165°E (Wijffels 1993) to 110°W (Hayes and Milburn 1980); zonal velocities are coherent over at least 10° of longitude (1200 km) (Ponte and Luyten 1989). The jets migrate slowly in time if at all;over 16 months of observations, they have been observed to migrate at most 50 m vertically (Firing 1987;Ponte and Luyten 1989).

There is no clear generation or forcing mechanism for the deep jets. Vertical internal instabilities have been explored, but no mechanism has yet been conclusively identified (L. Rothstein and S. Minobe 1996, personal communication; Rowe 1996). This paper explores the role that internal wave interactions play in maintaining the deep jets, but does not postulate a generation mechanism.

c. Internal wave field

The characteristics of the deep equatorial internal wave field are less well-defined than those of the mean flow field. There

is consistency with the spectral slopes of a Garrett–Munk spectrum modified for the equator (Munk 1981), but observations are scarce and show considerable temporal and spatial variability in spectral amplitude (Eriksen 1980; Hayes and Powell 1980; Hayes 1981; Blumenthal 1987; Gregg et al. 1996). In addition, most observations of the internal wave field are taken at the equator where the deep jets influence the local internal wave dynamics.

The equatorial vertical wavenumber spectrum is enhanced over that of midlatitudes for vertical wavelengths $300 < \lambda_z < 10$ m (Hayes and Powell 1980). In all cases, the frequency dependence of the spectra is close to ω^{-2} and the vertical wavenumber dependence, m^{-2} (Hayes 1981; Blumenthal 1987; Gregg et al. 1996). Vertical displacement spectra approximately follow an equatorially enhanced Garrett–Munk spectrum, although spectral levels are not constant on timescales of months. Spatial and temporal variance in spectral levels are comparable to those seen at midlatitudes.

Frequency spectra indicate a continuous spectrum of wave activity, with Kelvin and mixed Rossby–gravity waves dominating the lower frequencies and a transition to inertial gravity waves at periods of roughly one week (Eriksen 1980). Blumenthal (1987) also found that an equatorially enhanced GM spectrum models equatorial spectra adequately. Lower frequency motions ($\omega < 2 \times 10^{-4}$ rad s^{-1}) are slightly less energetic than predicted by a GM spectrum, and his model fit could be improved by accounting for horizontal and vertical anisotropy and the effects of mean shear (Blumenthal 1987). In the absence of a better model of internal wave energy for the tropical oceans, we use the Garrett–Munk spectrum to describe the local internal wave field.

d. Energy transfer at critical layers

We described the mean background field of the deep jets in section 1b and the perturbation field of the internal waves in section 1c. As a next step, a theory must be developed to understand how the wave field influences the mean flow. Under the noninteraction theorem, there can be no acceleration of a mean flow by a linear, inviscid, nonlocally forced, harmonic wave field in the absence of critical layers (Eliassen and Palm 1961). Therefore, the deep equatorial internal wave field primarily effects the deep jets through critical-layer interactions. We assume friction away from the critical layer is small; frictional effects due to the observed enhanced dissipation rates are discussed by Muench and Kunze (MK99). We do not speculate on the exact nature of the critical layer, where the wave either breaks or decomposes into smaller vertical scales through wave–wave interactions, but note that little wave energy appears to propagate away from critical layers (Kunze et al. 1995).

Internal wave energy will be partitioned between that transferred to the mean through momentum-flux divergence and that lost to turbulence. In a Lagrangian frame, all energy is lost to dissipation. This is the intrinsic energy associated with the intrinsic frequency, $E_I = A/\omega_I$, where A is the wave action. We can also calculate the energy in an Eulerian frame using the relation $E_E = E_I + \mathbf{U} \cdot \mathbf{k}A$ (Henyey and Pomphrey 1983). Noting that the wave momentum can be expressed as $\mathbf{p} = A\mathbf{k}$, then to conserve momentum, energy transferred to the mean flow must be $E_E - E_I = \mathbf{U} \cdot \mathbf{p} = \mathbf{U} \cdot \mathbf{k}E_I/\omega_I$ (Henyey et al. 1986). By estimating the magnitude and structure of the momentum-flux divergence, we model acceleration of a mean flow due to internal waves.

e. Spectral replenishment

Critical-layer interactions with the jets will deplete the internal wave spectrum at short vertical wavelengths. However, depletion is not observed in the deep equatorial ocean, suggesting that spectral replenishment through wave–wave interactions restores the internal wave field toward GM levels. Considerations of spectral replenishment have not been included in previous estimates of momentum-flux divergence from internal wave interactions with sheared flows. They prove to be of paramount importance in this study.

The theory of wave–wave interactions and how they shape the midlatitude spectrum has been widely investigated (McComas and Bretherton 1977; McComas and Müller 1981; Henyey and Pomphrey 1983; Müller et al. 1986). These studies conclude that nonlinear wave–wave interactions are an important link in the energy cascade from large to small scales and may be responsible for several characteristics of the GM spectrum such as the smoothness at high wavenumbers, vertical symmetry, and the inertial peak. These theories find that the GM spectrum is an equilibrium spectrum for the internal wave field; any depletion or excess of energy at a given frequency or vertical wavenumber is smoothed out over some relaxation timescale (McComas and Müller 1981). There is still some controversy over the exact mechanisms governing the relaxation timescale and rate of replenishment (reviewed in Müller et al. 1986).

It is unclear how to extend midlatitude theories of spectral replenishment to the equator. The internal wave band on the equator is broader, allowing higher internal wave shear than at midlatitudes. However, background equatorial turbulence levels are no higher than those at midlatitudes, suggesting slower wave–wave interaction timescales (Gregg et al. 1995). The presence of a sheared mean flow with a vertical wavelength of just 330 m (comparable to much of the internal wave field) may also impact which waves result from wave–wave interactions, but this is not well addressed in the literature (Phillips 1968; Lelong and Riley 1991). In this paper, the theory of spectral replenishment is applied to establish its role in momentum-flux divergence of the internal wave field.

2. Model parameters

A general description of the background mean flow and local internal wave field are given above, as well as the theoretical framework for understanding how internal-wave critical layers will alter a sheared mean flow through momentum-flux divergences. This section outlines more precisely those parameters used in our model for momentum- and energy-flux divergences due to internal wave interactions with the deep jets. The spectral shape of the GM spectrum is discussed and restrictions due to WKBJ scaling of the wave–mean flow interaction defined.

a. Structure of the deep jets

The model deep jets are vertically sinusoidal and meridionally Gaussian, $U(y, z) = U_0 \exp[-y^2/(2L^2)] \cos(2\pi z/\Lambda)$, where L = 110 km is the equatorial radius of deformation. A Gaussian meridional structure incorrectly implies a Kelvin wave structure, while Muench et al. (1994) demonstrate that the jets are better described as long Rossby waves. However, critical-layer results are comparable for more realistic meridional structures. The vertical wavelength of the jets is chosen to be Λ = 330 m, corresponding to the average vertical wavelength of the Pacific deep jets (Muench et al. 1994). A case corresponding to the Atlantic jets, with a vertical wavelength Λ = 500 m, is discussed in connection with possibly shorter timescales of Atlantic and Indian jets (Böning and Schott 1993; O'Neill and Luyten 1984). The maximum jet velocity is U_0 = 5 cm s^{-1}.

b. The internal wave spectrum

An equatorially intensified GM model spectrum (Munk 1981) with energy levels set at 3°N is used to describe the energetics of the local internal wave field. We neglect low-frequency internal waves because they form meridional modes, inconsistent with our use of a WKB model (further discussed in section 2c). While equatorial intensification is observed, at high wavenumbers ($m > 0.08$ rad m^{-1}) levels are only 2–5 times the midlatitude estimates of GM76 (Hayes 1981; Gregg et al. 1995). The chosen spectral level agrees with observations to within a factor of 3, and we exclude from our model vertical wavenumbers higher than 0.6 rad m^{-1}. The exact form of the GM spectrum used in this estimate is presented in the appendix.

Several papers have investigated how dynamical differences between midlatitude and equatorial internal waves should influence the energy spectrum. Models including vertical shear produce the most realistic frequency spectra (Eriksen 1980, 1985; Blumenthal 1987) compared with observations. Changes in energy level can be included in the spectral level E_f and peak mode number j^*, which in our model are set at values appropriate to midlatitudes, $E_f = 4.6 \times 10^{-9}$ s^{-1} and j^* = 3. Changing the spectral level E_f changes the momentum- and energy-flux divergences by a comparable factor.

The GM spectrum has a rolloff at vertical wavenumbers above 0.6 rad m^{-1} (Gargett et al. 1981; Gregg and Kunze 1991). We restrict our estimate to lower vertical wavenumbers, assuming that motions of such short vertical wavelength do not contribute significantly to the momentum-flux divergence. Gregg et al. (1995) find equatorial shear spectra have rolloffs at lower wavenumbers (~ 0.3 rad m^{-1}) than midlatitudes and note that, despite the elevated internal wave shear of the equatorial region, turbulence is in general not enhanced. They conclude that the wave–wave interactions governing the evolution of the internal wave field may be different at low than midlatitudes. Effects of a lower rolloff on estimates will be discussed in the conclusions.

The derivation here assumes equipartition between internal waves of positive and negative vertical wavenumber. Observations have shown a slight net downward energy flux in the deep midlatitude ocean at near-inertial frequencies, most likely a signal of the downward energy flux from the surface (Leaman 1976; Müller et al. 1978). For the high wavenumbers of interest, minimum propagation times from the thermocline are 15 wave periods. At depth, finescale waves are more likely generated locally through processes that tend to make the spectrum vertically symmetric at high wavenumbers (Müller et al. 1986). Therefore, the assumption of equipartition of up- and downward energy is appropriate for the short vertical wavelengths ($\lambda_z < 80$ m) relevant to this problem.

c. WKBJ approximation

The limited vertical and meridional extent of the deep jets requires that the spectral estimate of internal wave energy be constrained by limiting the study to wavenumbers for which the WKBJ approximation is valid. To allow interactions within the WKBJ approximation, vertical wavelengths of the internal waves must be less than $\lambda_z \lesssim 80$ m ($|m| \geq 0.08$ rad m^{-1}). Relaxing this constraint to include all vertical wavenumbers would increase the momentum-flux divergence by at most a third.

To allow a WKBJ approximation in latitude, we require the meridional wavelength to be sufficiently short to allow a continuous spectrum of waves rather than the establishment of meridional modes. The limiting meridional mode number n for which this is valid is $1/[2(2n + 1)^2] \ll 1$ (Gill 1982); this expression is true for $n \geq 4$. Note that a meridional-mode-4 equatorial gravity wave with vertical wavelength $\lambda_z = 80$ m has a turning latitude (where $l = 0$) at 1.0°. We chose a minimum frequency of $\omega = 6.9 \times 10^{-6}$ rad s$^{-1} = f(3°N)$ (period of 10 days) to ensure this constraint. This further constrains the

horizontal wave angle, $\tan^{-1}(l/k) = \theta_{min} > 0.1$ rad ($=6°$). Smaller wave angles (low l and nearly zonal propagation) would establish meridional modes. The limit on frequency also removes waves with large wave angles (high l), which could interact with the deep jets, so our calculation may underestimate energy at low frequencies by up to a factor of 2. A constant $N = 2 \times 10^{-3}$ rad s^{-1} is assumed, consistent with the PEQUOD data ([Muench et al. 1994]).

d. Definition of critical vertical wavenumber

In considering the momentum-flux divergence, we need to determine which waves encounter critical layers in the deep jets. These will be defined by their initial vertical wavenumber as a function of mean zonal velocity. Only vertical critical layers will be considered here. Horizontal critical layers are possible for low-frequency waves, but their low vertical wavenumbers and high meridional wavenumbers result in relatively vertical ray paths that are more influenced by vertical than horizontal shear.

An internal wave encounters a vertical critical layer when

$$\omega_I = \omega_E - kU \rightarrow f, (3)$$

where ω_E is the Eulerian frequency of the wave (invariant regardless of Doppler shifting in a steady background flow) and ω_I the intrinsic frequency following the mean flow. To simplify notation and understanding, $\omega_0 = \omega_E$ is used to denote the intrinsic frequency of the wave at its initial position of 3°N where $U \approx 0$ m s^{-1} and where the intrinsic and Eulerian frequencies are equal.

The zonal wavenumber at which a wave encounters a vertical critical layer for any given U is $k = (\omega_0 - f)/U$. Using the relation between the zonal and vertical wavenumbers in the internal-wave dispersion relation, the critical vertical wavenumber is

$$m_i^{crit} = \frac{(\omega_0 - f)}{U_i \cos\theta} \left(\frac{N^2 - \omega_0^2}{\omega_0^2 - f^2} \right)^{1/2}, \qquad (4)$$

where θ is the orientation of the horizontal wavevector ($\theta > 6°$); $\theta = 0$ corresponds to a wave propagating eastward. Note that m_i^{crit} is the *initial* vertical wavenumber, that is, the vertical wavenumber of a ray at $U = 0$ that encounters a critical layer at zonal velocity U_i. This definition, in conjunction with the frequency limits defined below, is used quantify the momentum-flux divergence of internal waves interacting with the deep jets.

e. Frequency limits

The limits required by the WKBJ approximation necessitate bounds on frequency as well. The full range of frequencies (f, N) is not available for critical-layer interactions at all mean zonal velocities and wave angles. For a given $U \cos\theta$, [Fig. 2] shows m^{crit} from [(4)] as a function of frequency. The shaded region in [Fig. 2a and 2b] is an example of the portion of frequency/vertical wavenumber space interacts with the deep jets for the specific value of $U \cos\theta = 1$ and 2 cm s^{-1}, respectively. Other regions are excluded due to WKBJ considerations. Vertical wavenumbers $m < m^{crit}$ [dashed curves are m^{crit} for different values of $U \cos\theta$, calculated from [(4)]] do not encounter critical layers in the deep jets because the zonal wavenumber k is too low. To avoid violating our WKBJ conditions, we also restrict vertical wavenumbers $m > 0.08$ rad m^{-1} (dashed horizontal line). Combining these two restrictions places the following limits on the frequency interval that interacts with the deep jets as critical layers:

$$\omega_0 \geq \omega_f = f \left[1 + 2 \left(\frac{m^{min} U \cos\theta}{N} \right)^2 \right] \qquad (5)$$

and

$$\omega_0 \leq \omega_N = N \left[1 - \left(\frac{m^{min} U \cos\theta}{N} \right) \right]^{1/2}, \qquad (6)$$

where ω_N and ω_f are the intersection of m^{crit} with m^{min}. [Equations (5)] and [(6)] are solutions to [(4)] in the limits of $\omega_f \ll N$ and $\omega_N \gg f$, respectively. The dependence on $U \cos\theta$ follows from our definition of the critical vertical wavenumber [(4)]. It

is most restrictive on frequency for large mean zonal velocities and waves propagating parallel to the mean flow.

No WKBJ interaction between internal waves and mean flow occurs if $\omega_f \geq \omega_N$. This inequality holds for $U \cos\theta > 2.5$ cm s^{-1}, indicating that waves with zonal wavenumbers high enough to encounter a critical layer at this velocity have vertical wavelengths too long to permit the WKBJ approximation. In reality, critical-layer interactions undoubtedly occur for $U \cos\theta > 2.5$ cm s^{-1}, but cannot reliably be included in our linear model as they are outside the WKBJ limit of $\lambda_z < 80$ m. Since this is an energetic part of the internal wave spectrum, this limitation could reduce our estimate of momentum-flux divergence by a factor of 2. The maximum limit on vertical wavenumber, $m^{\max} = 0.6$ rad m^{-1}, is only important for $U \cos\theta < 0.2$ cm s^{-1}.

3. Calculation of momentum- and energy-flux divergences

Given the GM spectrum defined above and noting the restrictions due to the WKBJ approximation, momentum-flux divergences can be calculated by integrating over the vertical wavenumbers and frequencies that encounter critical layers with the deep jets. As waves stall due to critical-layer interactions, their momentum flux is transferred to the mean. To estimate the momentum-flux divergence, we calculate the difference in momentum flux between two points in space and take the limit as the distance between the points approaches zero.

Only the vertical momentum-flux divergence, $\partial\langle u'w'\rangle/\partial z$, is calculated. Similar methods may be used to estimate other components of momentum-flux divergence such as $\partial\langle u'\upsilon'\rangle/\partial y$ and $\partial\langle\upsilon'b'\rangle/\partial y$, but under equatorial scaling these do not contribute significantly to altering the mean flow.

a. Momentum-flux divergence along a ray path

The momentum flux at any given point can be estimated using the basic principles of ray tracing. We first assume that a full spectrum of internal waves is available to interact with the jets, regardless of interactions with adjacent jets. This is equivalent to assuming a single isolated jet. In general, not all rays are able to reach the center of the jets because they encounter critical layers on the edges of jets above and below, effectively shadowing the region between the jets from critical-layer interactions, an effect further discussed in section 4.

Figure 3 illustrates how a group of rays of identical initial frequency ω_0 and horizontal wavevector angle θ, but varying initial m, follow nearly the same path until a critical layer is approached. Each ray breaks at a certain zonal velocity U_i. Such a group of waves has a total vertical momentum-flux of $\langle u'w'\rangle_{\mathrm{TOT}}$. The magnitude of the momentum-flux $\langle u'w'\rangle_i$ at any location where the zonal velocity is U_i is reduced from that initial total as rays with higher vertical wavenumbers than m^{crit}_i encounter critical layers at mean zonal velocities smaller than U_i. Extending appropriate wavelengths to interact with the deep jets ($m^{\min} < m < m^{\max}$), we can describe the momentum-flux at any point as

$$\langle u'w'\rangle = \langle u'w'\rangle_{\mathrm{TOT}} - \frac{2b^2 E_0}{\pi}$$

$$\times \int_{0.1}^{\pi/2} \int_{\omega_f}^{\omega_N} \int_{m^{\min}}^{m_i^{\mathrm{crit}}} H(m, \theta)\, dm B_{uw}(\omega_0)\, d\omega_0\, d\theta,$$

$$(7)$$

where H and B_{uw} are the vertical wavenumber and frequency spectral shapes for the GM spectrum (appendix) and $E_0 = 4.6 \times 10^{-9}$ s^{-1}. The integral includes waves with vertical wavenumbers between the minimum available by WKB approximation and the critical wavenumber (4). The limits on frequency integration are ω_f and ω_N as defined in section 2e. The integration of horizontal wavenumber angle, including the factor of 2 in front, accounts for eastward propagating waves encountering critical layers in an eastward jet and excludes the interval [0, 0.1]; in a westward jet, the equivalent limits of integration are $\theta \in [\pi/2, \pi - 0.1]$.

The change in momentum-flux between two points along a ray with zonal velocities of U_i and U_{i-1}, respectively, is approximately

$$\text{(8)}$$

The differences between ω_f and ω_N at zonal velocities U_i and U_{i-1} is assumed small. The dependence on vertical wavelength can be expanded using (4),

$$\int_{m_i^{\text{crit}}}^{m_{i-1}^{\text{crit}}} H(m, \theta) \, dm$$

$$= -\frac{\pi j^*}{b} \frac{N}{N_0} \int_{m_i^{\text{crit}}}^{m_{i-1}^{\text{crit}}} \frac{dm}{(m + m^*)^2} \simeq \frac{\pi j^*}{b} \frac{N}{N_0} \left(\frac{1}{m_i^{\text{crit}}} - \frac{1}{m_{i-1}^{\text{crit}}} \right)$$

$$= -\frac{\pi j^*}{b} \frac{N}{N_0} \sqrt{\frac{\omega_0^2 - f^2}{N^2 - \omega_0^2}} \frac{(U_i - U_{i-1}) \cos\theta}{\omega_0 - f}.$$

We have neglected adjustment of the peak vertical wavenumber, $m^* = 9 \times 10^{-3}$ rad m^{-1} since m^* is low compared to the minimum vertical wavenumber available to interact with the equatorial deep jets, $|m| \geq 0.08$ rad m^{-1}.

The divergence of momentum-flux is the important quantity for investigating wave–mean flow interactions. To obtain the vertical divergence, we take the limit of (8) for infinitesimally small separations. In a continuous sense, (8) becomes

$$\frac{\partial \langle u'w' \rangle}{\partial z} = 2E_0 j^* b \frac{N}{N_0} \frac{\partial U}{\partial z}$$

$$\times \int_{0.1}^{\pi/2} \int_{\omega_f}^{\omega_N} B_{uw}(\omega_0) \sqrt{\frac{\omega_0^2 - f^2}{N^2 - \omega_0^2}} \frac{\cos\theta}{\omega_0 - f} \, d\omega_0 \, d\theta.$$

$$\text{(9)}$$

This includes downgoing waves encountering critical layers on the upper edge of a jet only.

UPWARD PROPAGATING WAVES

The momentum-flux divergence due to upward propagating waves is analogous to that of downward propagating waves by the symmetry of the jets. However, upward propagating waves have negative vertical wavenumbers, changing the sign of (9). Consequently, the momentum-flux divergence of an upward propagating wave is the exact opposite of a downward propagating wave, except for a factor to account for unequal energy partition, if appropriate.

Figure 4 ⬤ shows the difference in momentum flux between upward and downward propagating waves encountering critical layers in an isolated eastward jet with no replenishment of high-wavenumber waves. Eastward and downward propagating waves deposit negative momentum flux, while eastward and upward propagating wave deposit positive momentum flux. As downward propagating waves encounter critical layers for increasing values of mean zonal velocity, the magnitude of momentum flux decreases, becoming less negative until the waves reach the jet maximum, as shown in Fig. 4b ⬤ (solid curve). For upward propagating waves, the magnitude also decreases, becoming less positive (dashed curve). Figure 4c ⬤ shows the resulting net vertical momentum-flux divergence; the momentum-flux divergence is discontinuous at $U = 0$ and not smooth at the jet maximum. The discontinuity at $U = 0$ exists even in the presence of a continuous stack of jets because the zonal direction for waves encountering critical layers with jets switches at that point.

This vertical discontinuity of the momentum-flux divergence illustrates a contradiction in our assumption that only downgoing (upgoing) waves interact with the upper (lower) part of a jet. The contradiction is most apparent at $U = 0$, where the momentum contained in up- and downgoing waves should be equal and opposite in direction. By including spectral replenishment via wave–wave interactions in (9), a vertically continuous momentum-flux divergence is produced in section 4.

b. Estimating the momentum-flux divergence

With the above definitions, the momentum-flux divergence can now be estimated. A general expression for the momentum-flux divergence of a unidirectional wave field is

$$\frac{\partial}{\partial z}\langle u'w'\rangle = -C_{uw}(y, z)\left|\frac{\partial U}{\partial z}\right| \text{sgn}(U), \qquad (10)$$

where

$$C_{uw}(y, z) = 2E_0 j^* b \frac{N}{N_0} \int_{0.1}^{\pi/2} \int_{\omega_f}^{\omega_N} B_{uw}(\omega_0)\left(\frac{\omega_0^2 - f^2}{N^2 - \omega_0^2}\right)^{1/2}$$

$$\times \frac{\cos\theta}{\omega_0 - f} d\omega_0 \, d\theta. \qquad (11)$$

c. Dissipation

The energy-flux divergence is also an important quantity to investigate in a study of wave–mean flow interactions. While the momentum-flux divergence indicates where momentum is transferred from the internal wave field to the mean flow, the dissipation rate indicates where wave energy is lost to turbulence. The turbulent dissipation rate ε is measurable in the ocean, providing an observational check to theoretical estimates of the level of internal wave interactions with the deep jets.

The dissipation rate is the divergence of the energy flux $\varepsilon = |\nabla \cdot \mathbf{F}_I|$ due to critical-layer interactions of internal waves with the background mean flow ([Kunze et al. 1995](#)). As discussed in the introduction, the intrinsic energy of a wave is lost to turbulence at a critical layer since, in a Lagrangian frame, there is no background motion ([Henyey et al. 1986](#)). The energy-flux divergence of a wave is the change in energy-flux along a ray path where the energy flux is $\mathbf{F}_I = \langle \mathbf{v}'p'\rangle = \mathbf{C}_g E_I$, so

$$\varepsilon = \frac{\partial\langle v'p'\rangle}{\partial y} + \frac{\partial\langle w'p'\rangle}{\partial z} = \frac{\partial(C_{gy}E_I)}{\partial y} + \frac{\partial(C_{gz}E_I)}{\partial z}. \qquad (12)$$

This is easily calculated using the method derived to estimate momentum-flux divergences. Using definitions of the group velocity for an internal wave and the frequency dependence of the GM spectrum, an analogous argument may be made to that used in calculating the momentum-flux divergence. We find the vertical energy-flux divergence is

$$\frac{\partial}{\partial z}(C_{gz}E)$$

$$= 4E_0 j^* b\left|\frac{\partial(U^2)}{\partial z}\right| \int_{0.1}^{\pi/2} \int_{\omega_f}^{\omega_N} \frac{(\omega_I^2 - f^2)^{3/2}(\cos\theta)^2}{\omega_I^2(\omega_I - f)^2} d\omega \, d\theta, \qquad (13)$$

and the meridional energy-flux divergence is

$$\frac{\partial}{\partial y}(C_{gy}E)$$

$$= 2E_0 j^* b\left|\frac{\partial(U^2)}{\partial z}\right|$$

$$\times \int_{-\pi/2}^{\pi/2} \int_{\omega_f}^{\omega_N} \frac{(N^2 - \omega_I^2)^{1/2}(\omega_I^2 - f^2)(\cos\theta)^2}{\omega_I^2(\omega_I - f)^2} d\omega \, d\theta. \qquad (14)$$

The signs of both components of the energy-flux divergence are always positive since ε is a positive definite quantity. While the actual energy flux depends on the direction of the group velocity ([Fig. 4d](#) ⊙➡), the vertical divergence is everywhere positive. This is accounted for with the absolute values used in [(13)](#) and [(14)](#). The meridional component is included in our calculations, although it accounts for less than 10% of the total dissipation.

4. Model results

Precise values for the momentum- and energy-flux divergences can only be obtained numerically. We attempt to refine our estimate of the momentum-flux divergence by addressing the role of spectral replenishment of the internal wave field. If replenishment is instantaneous both between and within the jets, then there will be no net momentum-flux divergence. Some vertical anisotropy of the interval wave field is necessary for the existence of a nonzero net momentum-flux divergence. Here we explore the limits between no spectral replenishment and complete replenishment and discuss the role of the vertical wavelength of the jets.

Rays originating away from the deep jets encounter a critical layer on the edge of a jet, effectively shadowing the interior of adjacent jet from critical-layer interactions. This effect is illustrated in Fig. 5 ⊙, where rays with vertical wave angles steeper than S_+ or S_- ($S_\pm = \pm l/m$ are the slopes of the lines connecting the point in question with the maximum meridional extent of the isotach) encounter a critical layer with the upper jet before reaching the lower jet. The region between the jets should therefore be depleted of these steeper rays. Some energy in the internal wave band is replenished through wave–wave interactions. We explore the effects of our various assumptions by calculating both the momentum- and energy-flux divergences:

- with no replenishment,

- including replenished wave energy within each jet, and

- altering the vertical wavelength and replenishment rate.

The magnitude and structure of the momentum- and energy-flux divergences are discussed for each scenario.

a. No replenishment

We first investigate the magnitudes of the momentum- and energy-flux divergences with no spectral replenishment of shadowed rays between or within the deep jets by excluding all waves that would interact with an adjacent jet. Downgoing rays with y–z slopes greater than S_- and less than S_+ encounter a critical layer in a jet without critical-layer interaction with the jet above (Fig. 5 ⊙). Neglecting curvature of the U_i contour, where $U_i = U_0 \exp[-y^2_r/(2\Lambda^2)]$, the slopes of these lines are calculated assuming that the maximum (minimum) slope of a ray intersects the upper U_i contour at the minimum (maximum) y for that contour. Neglecting this curvature produces errors in the slope of less than 10% that, in turn, lead to uncertainties in the frequency cutoff of less than 10%. For northward(southward) propagating waves, the frequencies not influenced by shadowing from above are those such that

$$\omega_0 < \omega_{S_\pm} = \sqrt{\frac{S_\pm^2 N^2 + f^2 \sin^2\theta}{\sin^2\theta + S_\pm^2}}. \qquad (15)$$

The variables ω_{S-} and ω_{S+} are used to denote the equality of (15). In general, the slopes S_- and S_+ are small ($\sim 1 \times 10^{-4}$), so almost all frequencies $f < \omega_0 < N$ are shadowed.

Using the above limit on the frequency range, we estimate the momentum-flux divergence under conditions of no replenishment of depleted energy. Figure 6a ⊙ shows a contour plot of the resulting vertical momentum-flux divergence. The maximum is 1.5×10^{-8} m s^{-2}. The effect of shadowing is most pronounced in the center of the jets, and at the depth of the jet minimum ($U = 0$ cm s^{-1}) where the contour of constant mean zonal velocity is horizontal. The extremely small momentum-flux divergences in the center of the jets suggest that, without spectral replenishment, the internal wave field would be spectrally depleted of high-wavenumber waves within the deep jets. This result contradicts observations (Hayes and Powell 1980), and thus some spectral replenishment must occur between and within the deep jets.

Figure 6b ⊙ shows energy-flux divergence calculated with the same frequency limits. The largest energy-flux divergences (peak values of 6×10^{-10} m^2 s^{-3}) are not on the equator but centered at 0.5°N (and S). This level of energy dissipation would barely be noticeable above general oceanic dissipation and disagrees with dissipation rates of $O(10^{-9})$ W kg^{-1} observed on the equator in the Pacific and Atlantic at the depth of the deep jets (Gregg et al. 1995; K. Polzin 1996, personal communication). This strengthens our conclusion that some spectral replenishment must occur to allow the observed elevated dissipation rates and lack of spectral depletion in the observed internal wave field.

b. Internal wave energy replenishment between and within the jets

Having established the shadowed momentum-flux divergence in the absence of any wave regeneration between or within the jets, we now estimate how much energy can be replenished by wave–wave interactions. We calculate the time a ray takes to reach an adjacent jet for comparison with wave–wave interaction replenishment timescales. Following one of the trajectories shown in Fig. 5 ⊙, a ray starts just outside a region of critical U, heading toward a lower jet where the zonal

velocity again reaches a critical level. Moving along the ray, its energy gradually returns to GM levels as longer-vertical-wavelength internal waves interact with each other to replenish waves of short vertical wavelengths through parametric instabilities and induced diffusion (Müller et al. 1986). The travel time τ_t between the origin of the ray path and where that ray encounters a critical layer is estimated as

$$\tau_t \approx \int (dz/C_{gz}) \sim \Delta z/C_{gz},$$

where Δz is the vertical distance between identical isotachs in the two jets, and C_{gz} is taken to be a constant for the entire trajectory estimated at the depth where $U = 0$. This estimate fails to account for variation of both vertical wavenumber and intrinsic frequency over the ray path but suffices for a rough calculation. Ray tracing simulations show this estimate is off by a factor of 2 at most and is usually more accurate assuming a wave reaches a critical layer when its vertical wavelength reaches 10 m. However, slight modification of the critical wavenumber criterion produces large variations in the ray travel time. This contradiction is inherent in combining a ray-tracing approach with an ensemble description of the internal wave field. Altering the estimate of vertical group velocity would change the magnitude of our results, but not the structure, as discussed in the conclusions.

We assume that energy replenishment for any given frequency or vertical wavenumber occurs exponentially over the time period τ_t, so the energy of a ray at a critical layer can be estimated as

$$E(\omega, k_z) = (\tau_t/\tau_R)E_{TOT}(\omega, k_z)$$
$$= E_{TOT}(\omega, k_z)[1 - \exp(-2\nu_p\tau_t)], \quad (16)$$

where E_{TOT} is the estimated GM energy. A simplified value for the Langevin rate for induced diffusion is used,

$$\nu_p\tau_t = 6.4 \times 10^{-4}\frac{\Delta z N^2 m^2(\omega_0^2 - f^2)[H/(2\pi)]}{[1 - (\pi\omega_0/2N_0)]^6 f^2(N^2 - \omega_0^2)}$$

$$(17)$$

from Pomphrey et al. (1980), where H is the depth of the water column. As with all internal wave estimates in this model, $f(3°N)$ is used.

Accounting for energy replenishment in the momentum-flux divergence requires separation into several frequency bands according to local geometry. The slope and initial horizontal wavenumber angle of the wave, as well as the mean zonal velocity, determine which frequencies are shadowed, fully replenished, partially replenished, or unavailable to interact at any given point. The WKBJ limits of $\omega_0 \in [\omega_f, \omega_N]$ derived in section 2 still apply; for a given initial horizontal wavenumber angle θ, these are the only frequencies that can interact with a given zonal velocity U. Rays with frequencies $\omega_0 \in [\omega_f, \omega_{\pm S}]$ are unshadowed and therefore unaffected; all other frequencies have decreased energies. This information is summarized in Table 1 ⊙. Applying these constraints, the momentum-flux divergence at any point i is

$$\langle u'w'\rangle_i = \langle u'w'\rangle_{TOT} - \frac{E_0}{\pi}b^2\left(\int_{-\pi/2}^{-0.1}\int_{\omega_f}^{\omega_N}\int_{m^{min}}^{m_i^{crit}} H(m, \theta)\,dm B_{uw}(\omega_0)\,d\omega_0\,d\theta\right.$$
$$\mathrm{I}$$

$$-\int_{-\pi/2}^{-0.1}\int_{\omega_{S+}}^{\omega_N}\int_{m^{min}}^{m_i^{crit}} \exp(-2\nu_p\tau_t)H(m, \theta)\,dm B_{uw}(\omega_0)\,d\omega_0\,d\theta$$
$$\mathrm{II}$$

$$+\int_{0.1}^{\pi/2}\int_{\omega_f}^{\omega_N}\int_{m^{min}}^{m_i^{crit}} H(m, \theta)\,dm B_{uw}(\omega_0)\,d\omega_0\,d\theta$$
$$\mathrm{III}$$

$$\left.-\int_{0.1}^{\pi/2}\int_{\omega_{S-}}^{\omega_N}\int_{m^{min}}^{m_i^{crit}} \exp(-2\nu_p\tau_t)H(m, \theta)\,dm B_{uw}(\omega_0)\,d\omega_0\,d\theta\right). \quad (18)$$
$$\mathrm{IV}$$

(Click the equation graphic to enlarge/reduce size)

The range of horizontal wave angles is split between northward and southward propagating waves; the first two integrals

represent southward waves. The first and third integrals (I and III) are identical to (7). The second and fourth integrals (II and IV) remove from that total waves with only partially replenished energy.

The vertical momentum-flux divergence with shadowing and spectral replenishment is shown in Fig. 7a ⊙⁼. The maximum momentum-flux divergence is now 18×10^{-8} m s^{-2}. Comparing this value to the maximum of 1.5×10^{-8} m s^{-2} in Fig. 6a ⊙⁼ indicates that a significant portion of internal wave energy is replenished between the jets. The highest momentum-flux divergence is in the high shear layers between the jets. The structure is vertically discontinuous, and thus this estimate of momentum-flux divergence is not physically realistic.

The energy-flux divergence is also modified by spectral replenishment due to wave–wave interactions. The same limits on frequency as (18) apply. The shadowed regions have reduced energy-flux divergence due to incomplete spectral replenishment as shown in Fig. 7b ⊙⁼. The maximum energy-flux divergence is greater than the shadowed case by an order of magnitude and supports our supposition that significant replenishment of energy is necessary to explain the elevated dissipation rates observed in the shear zones between the deep jets (Gregg et al. 1995; K. Polzin 1996, personal communication).

c. Replenishment within a jet

So far we have only considered critical layers occurring as a wave moves into a jet. If the frequency spectrum is replenished in the low velocity regions between the jets, then replenishment of the spectrum through wave–wave interactions within the jets must also be considered. The momentum-flux divergence due to waves propagating out of jets will partially balance the flux-divergence associated with waves propagating into jets. Figure 5 ⊙⁼ illustrates the three types of waves included in this calculation.

Calculating the momentum-flux divergence inside a jet follows directly from calculation of momentum-flux divergence between the jets described in section 4b. In this case, all frequencies are shadowed with no dependence on the vertical slope of the ray path. The curvature of each U contour is neglected when calculating the thickness of the jet because meridional variation only is important for rays with angles from the vertical less than $\pi/100$. With this assumption, the distance between the contours of constant velocity is approximately $\Delta z \approx 2(z_i - z_c)$, where z_c is the depth of the jet maximum.

It is no longer logical to define the characteristics of waves as their value with no mean zonal velocity since the waves of interest are not physically realizable outside a mean flow. Instead, waves are defined by their characteristics at the jet maximum, $U = \pm 5$ cm s^{-1}, and $\omega_I = \omega_E - kU = \omega_0$. The zonal wavenumber of waves encountering critical layers is now in the same direction as U. For an unshadowed system, our estimate of the momentum-flux divergences (9) becomes

$$\frac{\partial \langle u'w' \rangle}{\partial z} = 2E_0 j^* b \frac{N}{N_0} \frac{\partial U}{\partial z} \int_{0.1}^{\pi/2} \int_{\omega_f}^{\omega_N} [1 - \exp(2\nu_p \tau_t)] B(\omega_0)$$

$$\times \sqrt{\frac{\omega_0^2 - f^2}{N^2 - \omega_0^2}} \frac{\cos\theta}{\omega_0 - f} d\omega_0 \, d\theta. \qquad (19)$$

The upper limit on frequency is that used in (18), our estimate of the replenished momentum-flux divergence, but the lower limit is ω_f rather than $\omega_{\pm S}$ because all frequencies within the jets are shadowed.

Figure 8a ⊙⁼ shows how the addition of momentum-flux divergence from waves generated inside the jets greatly decreases the total. Momentum-flux divergence from waves generated within each jet balances 90% of that generated between the jets. The maximum value is reduced by a factor of 10 and the vertical structure is continuous (Fig. 8a ⊙⁼). Momentum-flux divergence is a minimum at the jet centers and is small in regions of small mean zonal velocity between the jets. Although these are regions of high shear, the momentum-flux divergence due to waves generated within a jet completely cancels that generated between the jets. The momentum-flux divergence is not significantly larger than without spectral replenishment (Fig. 6a ⊙⁼), but the decrease is due to a more vertically isotropic rather than a depleted internal wave field.

While the momentum-flux divergence is cancelled when two otherwise identical waves encounter critical layers propagating vertically in opposite directions, the dissipation rate is doubled. Figure 8b ⊙⁼ shows the dissipation rate including replenishment within the jets. Values are in agreement with observations in the Pacific and Atlantic (Gregg et al. 1995; K. Polzin 1996, personal communication).

d. Jets with longer vertical wavelengths

Strong zonal currents have also been observed in the equatorial Indian (Luyten and Swallow 1976) and Atlantic Oceans (Ponte et al. 1990; J. Toole 1996, personal communication). Detailed estimates have not yet been made to determine their vertical wavelength, but preliminary measurements indicate longer vertical wavelengths than the Pacific jets, roughly 500 m.

To estimate the effect longer vertical wavelengths would have on the momentum-flux divergence, we model a jet with a 500-m vertical wavelength, decreasing the minimum vertical wavelength, $m^{\text{min}} = 0.05$ rad m^{-1}. The structure of the momentum-flux divergence remains the same, but the maximum value is half that of the shorter jet due to more complete spectral replenishment. The decrease in magnitude would be greater if we only increased the vertical wavelength of the jet. Expansion of the range of vertical wavenumbers available to interact with the jets counterbalances some of the reduction due to increased isotropy of the internal wave field.

5. Conclusions

Our model of spectral replenishment through wave–wave interactions indicates that the distances between the jets are sufficient for a significant fraction of the depleted internal wave band to be replenished. A large part of the finescale spectrum can also become replenished in the region within each jet. Including replenishment by wave–wave interactions both between and within the jets, we find vertically continuous momentum-flux divergences with maximum amplitudes of 1.8×10^{-8} m s^{-2} (=5 cm s^{-1}/month) and energy-flux divergences of 4×10^{-9} W kg^{-1}. The estimated energy-flux divergences are consistent with observed equatorial dissipation rates.

Model dependence on the vertical lengthscale of the deep jets indicates that the geometry of the deep jets has two important effects. First, under any given replenishment scheme, jets of longer vertical wavelengths have lower momentum-flux divergences as more of the spectrum can be replenished within each jet and so will more fully balance that generated between the jets. Second, some vertical anisotropy in the internal wave field is necessary to produce net momentum-flux divergences. Fortunately, the vertical wavelength of the Pacific jets is well established by the LIPP data (Fig. 1 ⬤▬); additional analysis of existing data is required to establish the vertical wavelength of the Atlantic deep jets.

a. Implications

The magnitude of the momentum-flux divergence from the most realistic of our models—including shadowing and replenishment both between and within the deep jets—is 1.8×10^{-8} m s^{-2}. In section 4, we postulated a balance $\partial \tilde{\mathbf{u}}/\partial t = -\langle u'w'\rangle_z$, where $\tilde{\mathbf{u}}$ is the flow forced by the momentum-flux divergence. Having quantified the momentum-flux divergence $\langle u'w'\rangle_z$, the wave-driven acceleration can be as large as 1 cm s^{-1} week. This value is large compared with the observed 5 cm s^{-1} mean maximum velocity of the jets and calls into question the model assumptions. These are addressed next.

b. Assumptions

Our model of the momentum-flux divergence is based on a large number of assumptions concerning the dynamics of the deep ocean. The major points that require attention are

- the travel time of rays in shadowed zones can be estimated from the group velocity based on no mean flow,

- the replenishment rate remains constant over the path of a ray,

- the magnitude of the internal wave field available to interact with the deep jets, and

- the deep jets are the only background flow.

Our first assumption is that we can estimate the travel time of a ray propagating through a sheared flow using the frequency, vertical wavenumber, and group velocity calculated at a point with no mean flow. This assumption is problematic considering that the vertical group velocity can change by at least an order of magnitude over a ray path. In addition, the travel time approaching a critical layer is theoretically infinite. In all of our estimates we have chosen a vertical wavelength cutoff of 10 m to avoid the rolloff region of the internal wave spectrum (Gregg et al. 1995). We calculated the travel time for several rays in a shadow zone between the jets and found our estimate to be correct to within a factor of 2. However, a reduction of a few meters in the choice of vertical cutoff greatly increases the travel time, so the choice of 10 m may be serendipitous. A dependence on vertical wavenumber cutoff calls into question the spectral replenishment estimate.

Under(over)-estimate of the vertical group velocity would increase (decrease) the magnitude of the momentum-flux divergence. However, the structure of the momentum-flux divergence would not be significantly altered and would still only be significant in limited areas on the edges of the jet maxima.

Our use of a constant spectral replenishment rate over the path of a ray is at best a rough guess. A more accurate model would allow the replenishment rate to vary with frequency and vertical wavenumber (Müller et al. 1986). However, calculating the replenished energy for the entire frequency/wavenumber spectrum at every point within the jets would be computationally prohibitive.

Gregg et al. (1995) suggest spectral replenishment may be slower at low than at midlatitudes. A slower replenishment rate would increase the magnitude of the momentum-flux divergence by restocking the depleted wave field between and within the jets less. Altering the replenishment rate primarily influences the magnitude of the momentum-flux divergence, not the

dipolar structure nor the magnitude of the energy-flux divergence.

The magnitude of the internal wave field energy available to interact with the deep jets varies spatially and temporally by a factor of 3. This variation would alter the momentum-flux divergences by the same degree over periods of a few months. In addition, we have limited the frequency range to exclude waves of meridional mode $n \lesssim 4$. As discussed in <u>section 2c</u>, this limit could underestimate the momentum-flux divergences by a factor of 2.

An effect of the momentum-flux divergence that is even harder to estimate is that of interactions between internal waves and shear flows other than deep jets. The deep equatorial ocean contains a plethora of equatorially trapped and other strong vertical shears with periods ranging from 2 weeks to 2 years. <u>Ponte and Luyten (1989)</u> find significant peak energy at 560 sm (stretched meters), well removed from the peak associated with the deep jets. Both peaks lie above an energetic spectrum. Elevated dissipation levels in high shear zones on the equator occur not just between the deep jets but anywhere the vertical shear of the meridional velocity is large as well (M.C. Gregg 1996, personal communication). Internal wave interactions with other shears will weaken the momentum-flux divergence because of the more random distribution of critical-layer interactions.

If the replenishment rate is slow, then a sizeable percentage of the internal wave field encounters critical-layer interactions with motions other than the jets, thereby greatly decreasing the amount of energy available to interact with the deep jets. Quantifying this effect is difficult. <u>Ponte and Luyten (1989)</u> estimated that the deep jets account for roughly 20% of the total variance in the vertical wavenumber spectrum. If only 20% of the finescale internal wave field interacts with the deep jets and the remaining 80% interacts with other sheared flows, then the vertical momentum-flux divergence would reach a maximum of 3×10^{-9} m s^{-2} = 9 cm s^{-1}/yr.

We emphasize that all the assumptions we have discussed above alter the magnitude of the momentum-flux divergence but not the structure. Despite uncertainties in the spectral replenishment scheme, the following conclusions are robust under other models of spectral replenishment:

- momentum-flux deposition is confined to the high shear layers between the jets,

- observed dissipation rates require some spectral replenishment, and

- as long as spectral replenishment is not instantaneous, there is a vertical momentum-flux divergence associated with the deep jets.

The magnitude and structure of the accelerations that result from our estimate of momentum-flux divergence remain to be explored, but from rough calculations small momentum-flux divergences could result in large accelerations of the mean flow.

REFERENCES

Blumenthal, M. B., 1987: Interpretation of equatorial current meter data as internal waves. Ph.D. dissertation, WHOI, Woods Hole, MA, 371 pp. [Available from WHOI, Woods Hole, MA 02453.].

Böning, C. W., and F. A. Schott, 1993: Deep currents and the eastward salinity tongue in the equatorial Atlantic: Results from an eddy-resolving, primitive-equation model. *J. Geophys. Res.,* **98,** 6991–6999..

Eliassen, A., and E. Palm, 1961: On the transfer of energy in stationary mountain waves. *Geophys. Publ.,* **22,** 409–418..

Eriksen, C. C., 1980: Evidence for a continuous spectrum of equatorial waves in the Indian Ocean. *J. Geophys. Res.,* **85,** 3285–3303..

—— ,1985: Some characteristics of internal gravity waves in the equatorial Pacific. *J. Geophys. Res.,* **90,** 7243–7255..

Firing, E., 1987: Deep zonal currents in the central equatorial Pacific. *J. Mar. Res.,* **45,** 791–812..

—— ,1988: Shallow equatorial jets. *J. Geophys. Res.,* **93,** 9213–9222..

Gargett, A. E., P. J. Hendricks, T. B. Sanford, T. R. Osborn, and A. J. Williams III, 1981: A composite spectrum of vertical shear in the upper ocean. *J. Phys. Oceanogr.,* **11,** 1258–1271.. <u>Find this article online</u>

Gill, A. E., 1982: *Atmosphere–Ocean Dynamics.* Academic Press, 662 pp..

Gregg, M. C., D. P. Winkel, T. B. Sanford, and H. Peters, 1995: Turbulence produced by internal waves in the oceanic thermocline at mid- and low-latitudes. *Dyn. Atmos. Oceans,* **24,** 1–14..

Hayes, S. P., 1981: Vertical fine structure observations in the eastern equatorial Pacific. *J. Geophys. Res.,* **86,** 10 983–10 999..

—— , and H. B. Milburn, 1980: On the vertical structure of velocity in the eastern equatorial Pacific. *J. Phys. Oceanogr.,* **10,** 633–635.. Find this article online

—— , and C. J. Powell, 1980: Vertical wave number spectra of temperature fine structure in the equatorial Pacific. *J. Geophys. Res.,* **85,** 4029–4035..

Henyey, F. S., and N. Pomphrey, 1983: Eikonal description of internal wave interactions: A non-diffusive picture of "induced diffusion." *Dyn. Atmos. Oceans,* **7,** 189–219..

—— , J. Wright, and S. M. Flatte, 1986: Energy and action flow through the internal wave field: An eikonal approach. *J. Geophys. Res.,* **91,** 8487–8495..

Kunze, E., and P. Müller, 1989: The effect of internal waves on vertical geostrophic shear. *Parameterization of Smallscale Processes, Proc. 'Aha Huliko'a Hawaiian Winter Workshop,* Hawaii Inst. Geophys. Spec. Publ., 271–285..

—— , R. W. Schmitt, and J. M. Toole, 1995: The energy balance in a warm-core ring's near-inertial critical layer. *J. Phys. Oceanogr.,* **25,** 942–957.. Find this article online

Leaman, K. D., 1976: Observations of vertical polarization and energy flux of near-inertial waves. *J. Phys. Oceanogr.,* **6,** 894–908.. Find this article online

Lelong, M. P., and J. R. Riley, 1991: Internal wave-vortical mode interactions in strongly stratified flows. *J. Fluid Mech.,* **232,** 1–19..

Luyten, J. R., and J. C. Swallow, 1976: Equatorial undercurrents. *Deep-Sea Res.,* **23,** 999–1001..

McComas, C. H., and F. P. Bretherton, 1977: Resonant interaction of oceanic internal waves. *J. Geophys. Res.,* **82,** 1397–1412..

—— , and P. Müller, 1981: Time scales of resonant interactions among oceanic internal waves. *J. Phys. Oceanogr.,* **11,** 140–147.. Find this article online

Muench, J. E., E. Kunze, and E. Firing, 1994: The potential vorticity structure of equatorial deep jets. *J. Phys. Oceanogr.,* **24,** 418–428.. Find this article online

Müller, P., D. J. Olbers, and J. Willebrand, 1978: The IWEX spectrum. *J. Geophys. Res.,* **83,** 479–500..

Müller, P., G. Holloway, F. Henyey, and N. Pomphrey, 1986: Nonlinear interactions among internal gravity waves. *Rev. Geophys.,* **24,** 493–536..

Munk, W., 1981: Internal waves and small-scale processes. *Evolution of Physical Oceanography,* B. A. Warren and C. Wunsch, Eds., The MIT Press, 264–291..

O'Neill, K., and J. R. Luyten, 1984: Equatorial velocity profiles. Part II: Zonal component. *J. Phys. Oceanogr.,* **14,** 1842–1852.. Find this article online

Phillips, O. M., 1968: The interaction trapping of internal gravity waves. *J. Fluid Mech.,* **34,** 407–416..

Pomphrey, N., J. D. Meiss, and K. M. Watson, 1980: Description of nonlinear internal wave interactions using Langevin methods. *J. Geophys. Res.,* **85,** 1085–1094..

Ponte, R. M., and J. Luyten, 1989: Analysis and interpretation of deep equatorial currents in the central Pacific. *J. Phys. Oceanogr.,* **19,** 1025–1038.. Find this article online

—— , —— , and P. L. Richardson, 1990: Equatorial deep jets in the Atlantic Ocean. *Deep-Sea Res.,* **37,** 711–713..

Reynolds, O., 1895: On the dynamical theory of incompressible fluids and the determination of the criterion. *Philos. Trans. Roy. Soc. London,* **A186,** 123..

Rowe, D., 1996: Eddy forcing of subthermocline equatorial mean flow. Ph.D. dissertation, University of Rhode Island, Narragansett, RI, 98 pp. [Available from University of Rhode Island, Narragansett, RI 02882.].

Ruddick, B. R., and T. M. Joyce, 1979: Observations of interaction between the internal wavefield and low-frequency flows in the North Atlantic. *J. Phys. Oceanogr.,* **9,** 498–517.. Find this article online

Wijffels, S. E., 1993: Exchanges between hemispheres and gyres: A direct approach to the mean circulation of the equatorial Pacific. Ph.D. dissertation, WHOI, Woods Hole, MA, 267 pp. [Available from WHOI, Woods Hole, MA 02543.].

APPENDIX A

6. The Garrett–Munk Spectrum

The GM spectrum can be expressed as

$$_{GM}S_\zeta(\omega, m) = b^2 \frac{N_0}{N}\left(\frac{\omega^2 - f^2}{\omega^2}\right) E(\omega, m), \qquad (A1)$$

$$_{GM}S_u(\omega, m) = b^2 N_0 N\left(\frac{\omega^2 + f^2}{\omega^2}\right) E(\omega, m), \qquad (A2)$$

where

$$E(\omega, m) = \frac{E_0}{f}B(\omega)H(m), \qquad (A3)$$

the energy parameter $E_0 = 4.6 \times 10^{-9}$ s^{-1}, f is set at $f(3°N) = 7.6 \times 10^{-6}$ s^{-1}, and the stratification scale $b = N/N_z = 1300$ m. The GM frequency functions for horizontal and vertical velocity, and buoyancy are

$$B_\perp(\omega_0) = N_0 N\frac{f^2}{\omega_0^3\sqrt{\omega_0^2 - f^2}},$$

$$B_\|(\omega_0) = N_0 N\frac{1}{\omega_0\sqrt{\omega_0^2 - f^2}} \qquad (A4)$$

$$B_w(\omega_0) = \frac{N_0}{N}\frac{\sqrt{\omega_0^2 - f^2}}{\omega_0},$$

$$B_b(\omega_0) = N_0 N^3\frac{\sqrt{\omega_0^2 - f^2}}{\omega_0^3}. \qquad (A5)$$

Horizontal velocity is separated into the components perpendicular and parallel to the horizontal wavenumber angle, θ, $u = u_\|\cos\theta - u_\perp\sin\theta$; $v = u_\|\sin\theta + u_\perp\cos\theta$. The vertical wavenumber dependence is

$$H(m) = \frac{\pi j^*}{b}\frac{N}{N_0}\frac{1}{(m + m^*)^2}. \qquad (A6)$$

We have chosen a vertical mode number $j^* = 3$, which at midlatitudes contains the peak kinetic energy and corresponds to $m^* \approx 9 \times 10^{-3}$ rad m^{-1} ($\lambda^*_z = 700$ m).

Tables

Table 1. Variables.

| Variable	Definition	Reference
ω_f	Lower frequency limit due to WKB scaling	(5)
ω_N	Upper frequency limit due to WKB scaling	(6)
ω_{zs}	Upper frequency limit on waves not shadowed	(15)
τ_t	Travel time between jets	$\Delta z/C_{gz}$
ν_p	Lagevin replenishment rate	(17)
$m^{cm}(i)$	Initial vertical wavenumber of wave encountering a critical layer at i	(4)
θ_{min}	0.1 rad, minimum horizontal wavenumber to avoid establishment of meridional modes	Section 1c

Click on thumbnail for full-sized image.

Figures
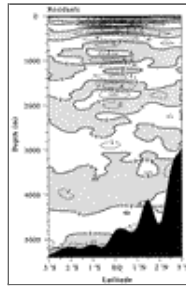
Click on thumbnail for full-sized image.

Fig. 1. Meridional structure of the residual mean zonal currents. To separate the deep jets from the larger vertical scale structure, the 16-month mean zonal velocity field has been decomposed into a low-mode component (not shown) and a high-mode residual (Firing 1988). The deep jets are constrained to the equator and have an average vertical wavelength of 330 m.
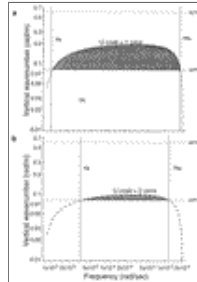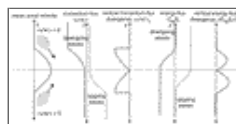

Click on thumbnail for full-sized image.

Fig. 2. Critical vertical wavenumber as a function of frequency for different values of $U \cos\theta$ (cm s^{-1}). On each plot, horizontal lines mark $m^{min} = 0.08$ rad m^{-1}, the lowest wavenumber available to interact with the deep jets under WKB scaling and $m^{max} = 0.6$ rad m^{-1}, the GM spectral rolloff. The region highlighted in gray signifies frequencies and vertical wavenumbers available to encounter critical layers for this value of mean zonal velocity and horizontal wave angle. In (a) and (b), the frequency limits ω_f and ω_N are defined as the frequencies at which $m = 0.08$ rad m^{-1} intersects the $U \cos\theta = 1$ cm s^{-1} and 2 cm s^{-1} lines, respectively.
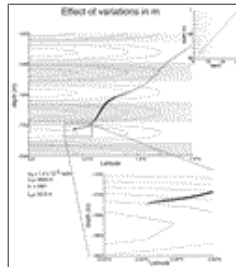
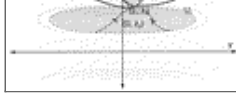Click on thumbnail for full-sized image.

Fig. 3. Rays of the same initial frequency, horizontal wavevector angle and initial position but different initial vertical wavenumbers follow the same path in a southwesterly direction until a critical level is reached in an eastward jet. The lower inset shows in detail how the rays reach a critical layer. The inset on the upper right shows the large-scale view, including the initial position of the rays. Gray shading indicates westward flow. Contour intervals are ±1, 2, and 4 cm s^{-1} in the large view and 0.2 cm s^{-1} in the lower detailed view. Initial vertical wavelength varies from 33.1 to 35.3 m.

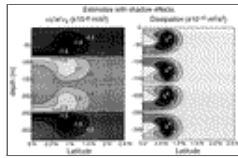
Click on thumbnail for full-sized image.

Fig. 4. Schematic of momentum-flux divergence at an isolated eastward jet. The mean zonal velocity with depth is shown in (a). The momentum-flux (b) only changes where the zonal velocity changes. The solid line is the momentum-flux divergence for downward-propagating waves, the dashed upward. The momentum-flux divergence (c) is vertically discontinuous. The vertical component of the energy-flux (d) is also in the opposite direction for up- and downgoing waves, but its vertical divergence (e) is always positive definite.

Fig. 5. Ray paths in shadow zones. Arrows show the direction of propagation. The black dashed ovals are contours of constant zonal velocity U_i, and (y_i, z_i) is the point where the rays encounter a critical layer. The three ray types are (i) those originating from the shadowed zone between the jets (dashed downgoing rays), (ii) rays generated within the lower jet (dashed upgoing rays), and (iii) rays uninfluenced by the presence of adjacent jets (solid downgoing rays).

Fig. 6. Energy dissipation due to internal waves reaching critical layers in the deep jets, including the effects of shadowing by adjacent jets. Dissipation is reduced by an order of magnitude from estimates without adjacent jets, with a maximum of only 6×10^{-10} m^2 s^{-3} ($=W$ kg^{-1}). In addition, the highest dissipation rates are no longer at the equator, but are located at 0.5°N (and S).
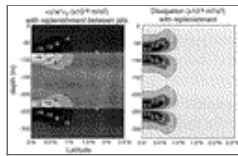
Fig. 7. Momentum-flux divergence estimated with the influence of shadowing by adjacent jets and spectral replenishment between the jets.
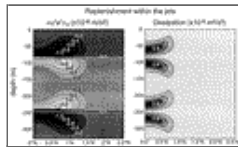
Fig. 8. Momentum-flux divergence estimated assuming influence of shadow effects between the jets and allowing spectral replenishment within each jet. The addition of momentum-flux divergence from waves generated within each jet balances a significant portion of the momentum-flux divergence.

Corresponding author address: Eric Kunze, APL, University of Washington, 1013 NE 40th, Seattle, WA 98105-6698. E-mail: kunze@ocean.washington.edu